Hongya SONG, Wenyi ZHANG, Haifeng LI, Xu LIU, Xiang HAO, 2020. Review of compact computational spectral information acquisition systems. *Frontiers of Information Technology & Electronic Engineering*, 21(8):1119-1133. https://doi.org/10.1631/FITEE.1900266

Review of compact computational spectral information acquisition systems

Key words: Spectral imaging; Computational imaging; Spectrometer

Corresponding author: Xiang HAO
E-mail: haox@zju.edu.cn
ORCID: https://orcid.org/0000-0002-3931-6884

Abstract

- In recent years, computational methods have been introduced into spectral detection, and computational spectrum acquisition implementations have emerged.
- This paper highlights the advantages of computational spectrum acquisition implementations by comparing them with traditional non-computational methods. Then, focusing on the compact feature, we review the most representative implementations, and finally make discussion and offer an outlook.

Introduction

- In this review, we review many computational spectrometers and computational spectral imaging systems. We treat both systems as computational spectral information acquisition systems.

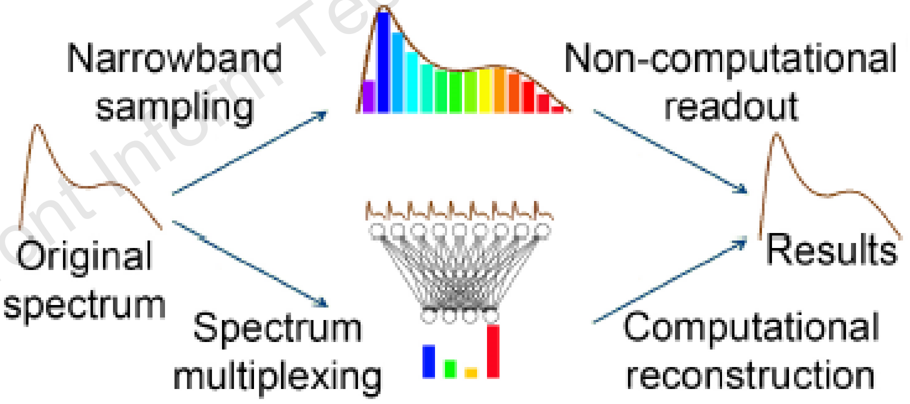

Fig. 1 Comparison of spectral detection using non-computational and computational methods

Computational spectrometers

1. Grating-based coded aperture spectrometer

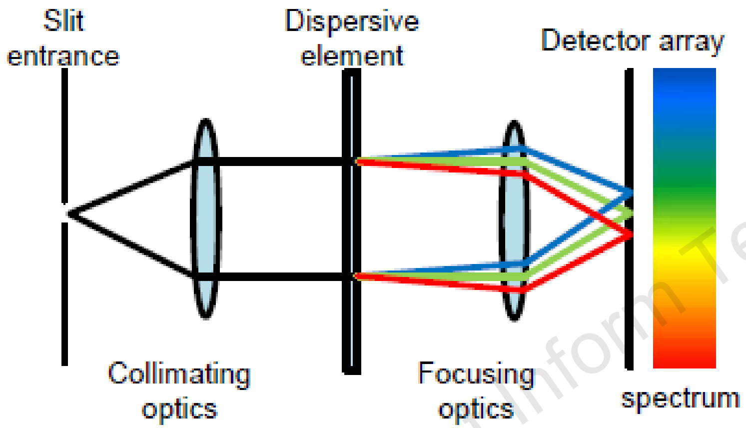

Fig. 2 Schematic of the traditional grating-based spectrometer

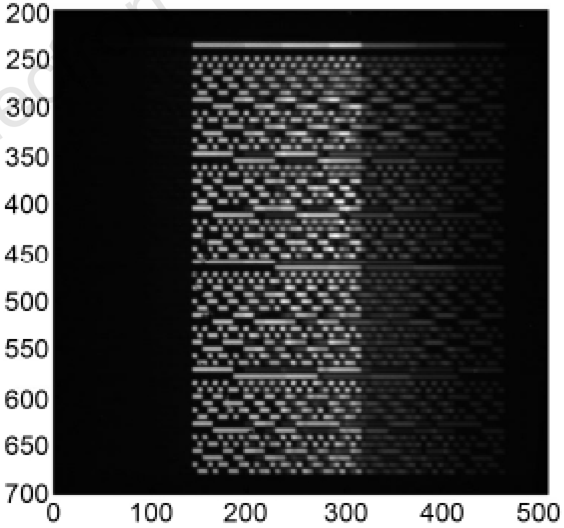

Fig. 3 Intensity image (distortion corrected) acquired by static MMS

Reprinted from Gehm et al. (2006), Copyright 2006, with permission from OSA

Computational spectrometers

1. Grating-based coded aperture spectrometer

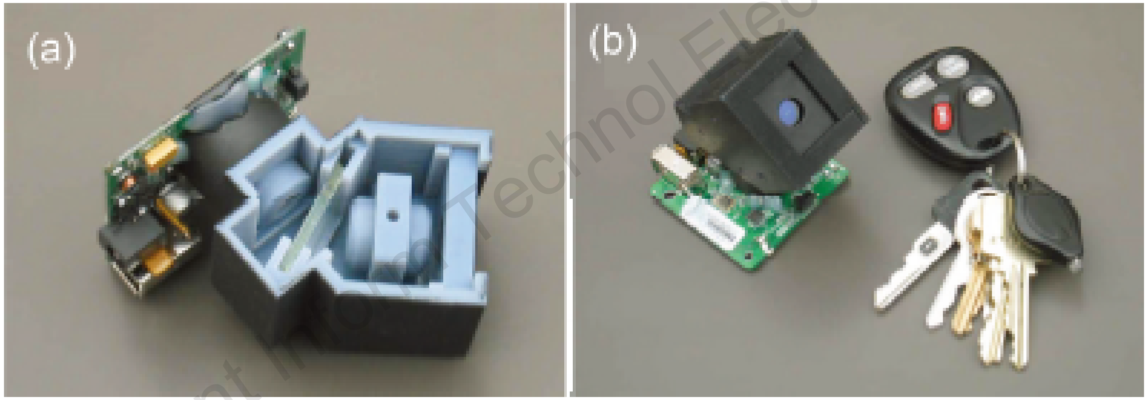

Fig. 6 Internal structure of the dispersion multiplexing spectrometer (DMS) (a) and DMS with keys to show the approximate size (b)

Reprinted from Cull et al. (2007), Copyright 2007, with permission from OSA

Computational spectrometers

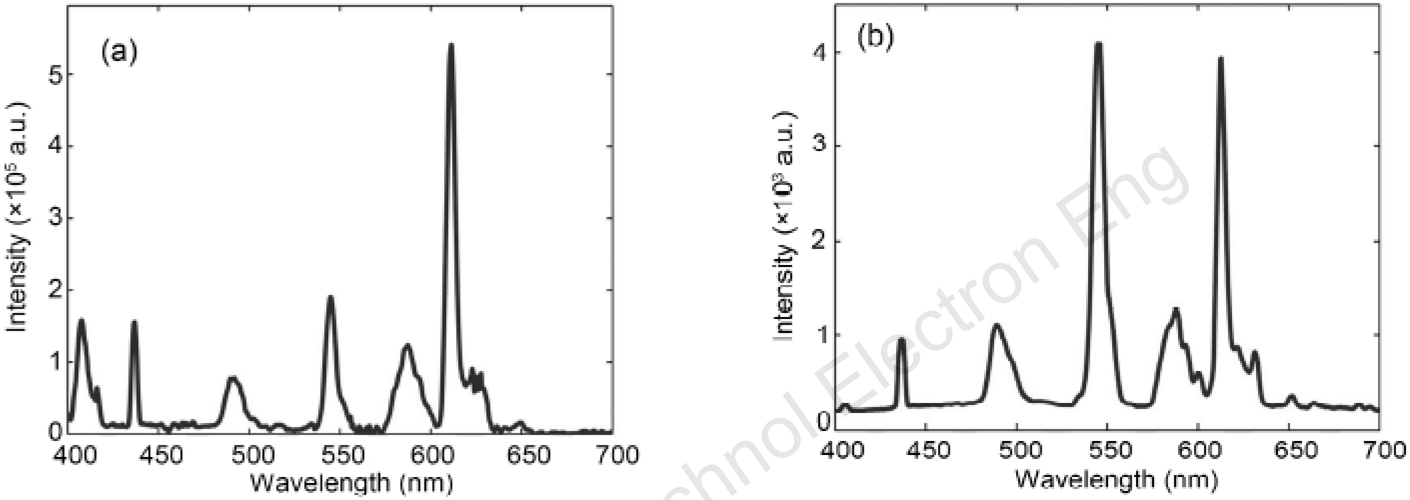

Fig. 4 Measurement result comparison between a dispersion multiplexing spectrometer (a) and a commercial spectrometer (b)

Reprinted from Cull et al. (2007), Copyright 2007, with permission from OSA

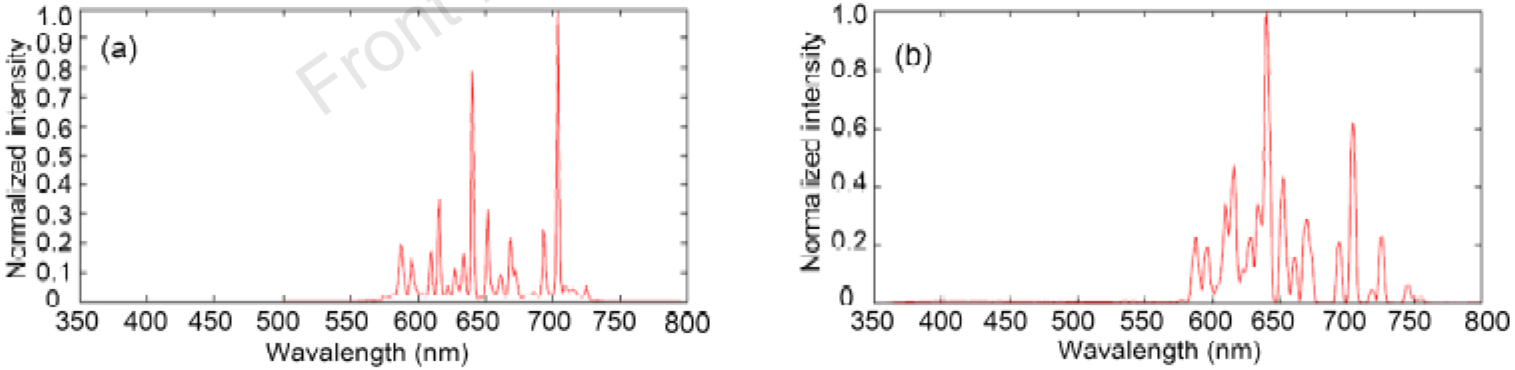

Fig. 5 Measurement results of a multi-order coded aperture (a) and a commercial spectrometer (b)

Reprinted from Feller et al. (2007), Copyright 2007, with permission from OSA

Computational spectrometers

2. Low-cost thin-film spectrometer

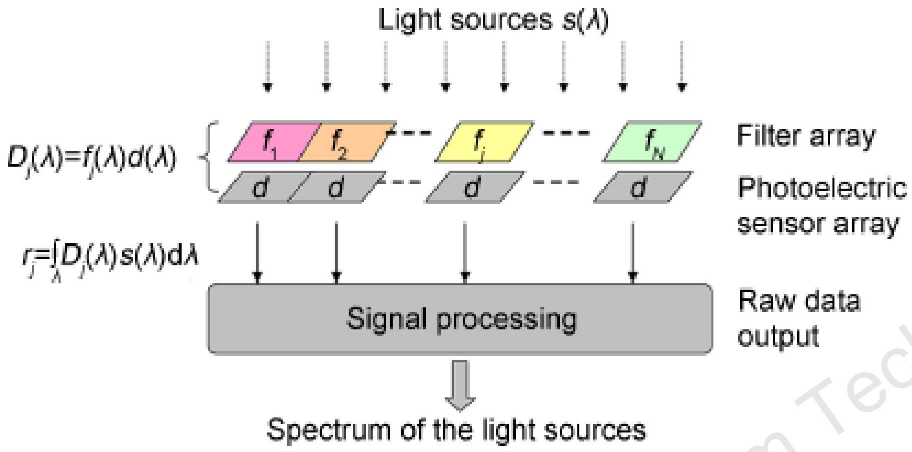

Fig. 7 Schematic of the filter array based spectrometer
Reprinted from Chang and Lee (2008), Copyright 2008, with permission from OSA

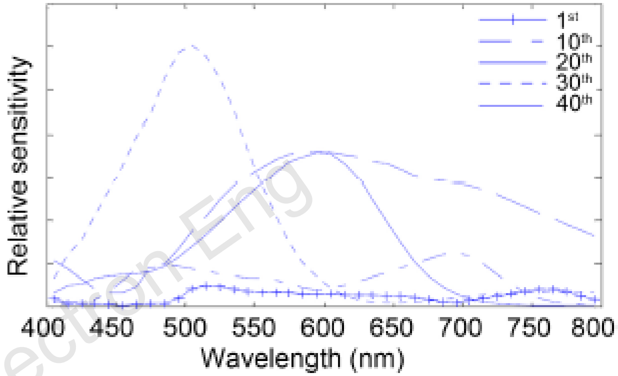

Fig. 8 Sensitivity responses of five spectral detectors among 40 low-cost filters
Reprinted from Chang and Lee (2008), Copyright 2008, with permission from OSA

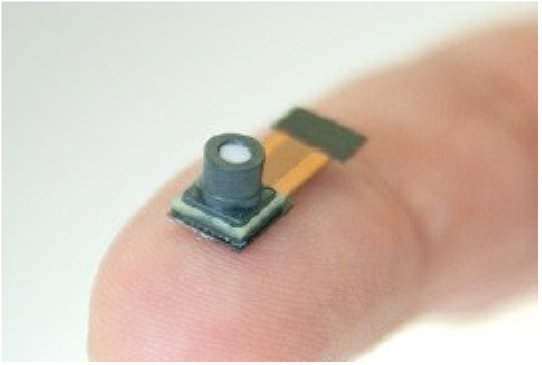

Fig. 9 Miniaturized spectrometer presented by Nano-Lambda Inc.
Reprinted from NanoLambda Inc. (https://nanolambda.myshopify.com), Copyright 2019, with permission from NanoLambda Inc.

Computational spectrometers

3. Etalon-based spectrometer

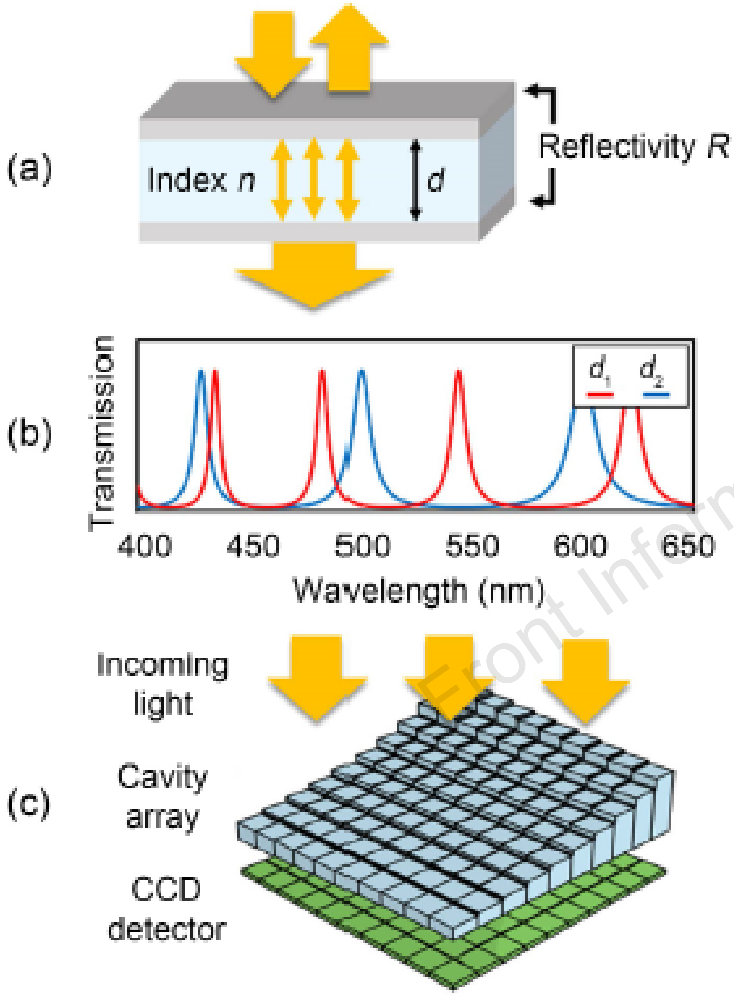

Fig. 10 System schematic of etalon-array reconstructive spectrometry: (a) an etalon consisting of two semireflecting surfaces with reflectivity *R* separated by an optically transparent medium of index *n* and thickness *d* (Light reflecting between the two surfaces interferes with itself, creating a characteristic transmission pattern); (b) two etalons of different thicknesses (d_1 and d_2) that will have uniquely encoded transmission patterns; (c) a CCD detector positioned under an etalon array with a unique thicknesses that will record the encoded light after it is transmitted through the etalons

Reprinted from Huang et al. (2017), Copyright 2017, with permission from Springer Nature, licensed under CC BY 4.0

Computational spectrometers

3. Etalon-based spectrometer

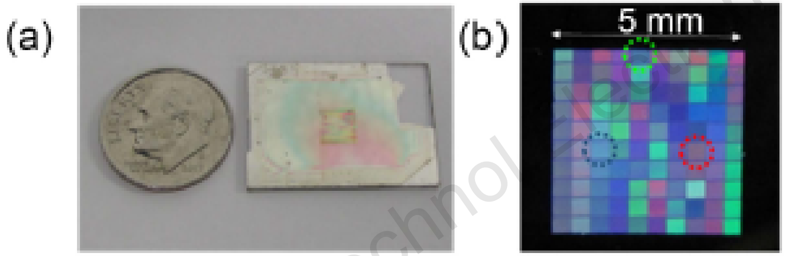

Fig. 11 Photograph of the cavity array in an etalon-array reconstructive spectrometry: (a) a photo of the fabricated 10×10 etalon array next to a dime for scale; (b) a color photograph of the etalon array back-illuminated by room fluorescent lighting, showing cavity-dependent color transmission

Reprinted from Huang et al. (2017), Copyright 2017, with permission from Springer Nature, licensed under CC BY 4.0

Computational spectrometers

4. Quantum dot spectrometer

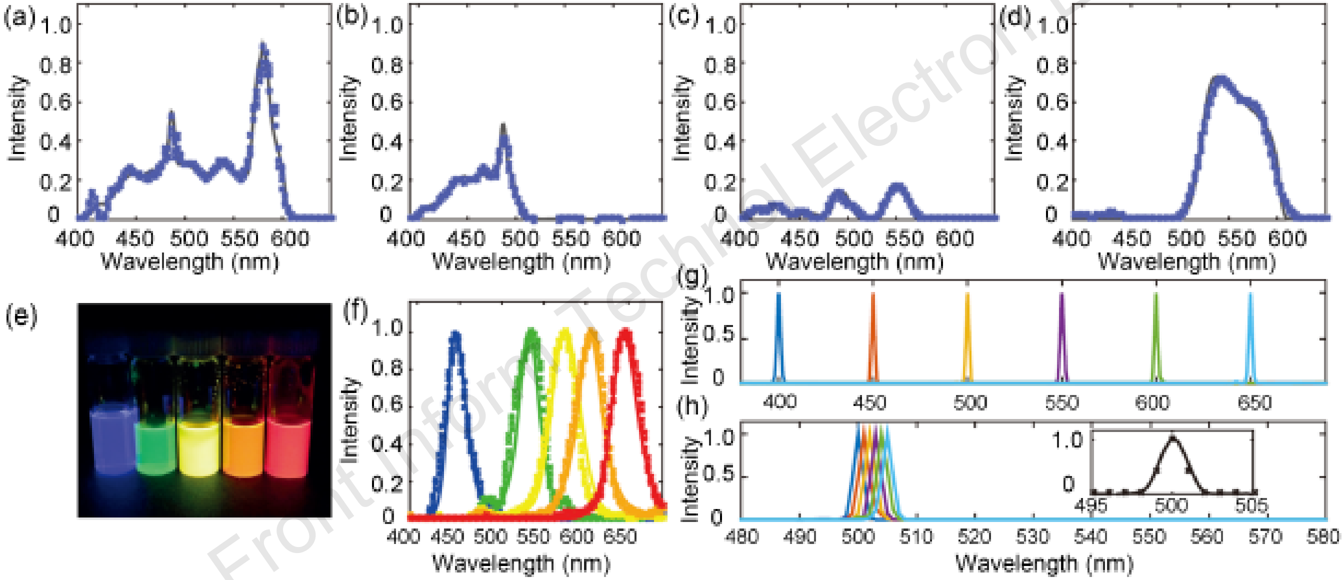

Fig. 12 Quantum dot spectrometer measurements: (a–d) quantum dot spectrometer measurements of broadband spectra (crosses) and reference spectra (solid lines) using a commercial spectrometer; (e) fluorescent emission of five CQD samples under ultraviolet excitation; (f) measurements (markers) using the quantum dot spectrometer of the emission spectra of the five CQD samples shown in (e), and reference spectra (solid lines) using a spectrofluorometer; (g, h) measurements of monochromatic light spectra

The peak positions of the six monochromatic lights in (g) are 400, 450, 500, 550, 600, and 650 nm. The peak positions of the six monochromatic lights in (h) are 500, 501, 502, 503, 504, and 505 nm. The inset of (h) compares the measured spectrum of the 500 nm monochromatic light with crosses and the reference spectrum with solid line. Reprinted from Bao and Bawendi (2015), Copyright 2015, with permission from Springer Nature

Computational spectrometers

4. Quantum dot spectrometer

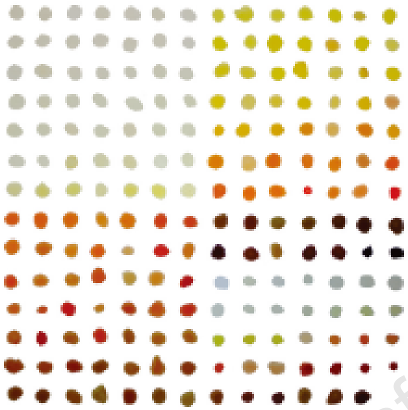

Fig. 13 Colloidal quantum dot (CQD) materials in the form of filters

Each dot is a CQD filter made of one type of CQD material embedded in a polyvinyl butyral thin film. Reprinted from Bao and Bawendi (2015), Copyright 2015, with permission from Springer Nature

Fig. 14 A quantum dot micro-spectrometer in the form of a digital camera with electronics and circuits

Reprinted from Bao and Bawendi (2015), Copyright 2015, with permission from Springer Nature

Computational spectrometers

5. Plasmonic metasurface spectrometer

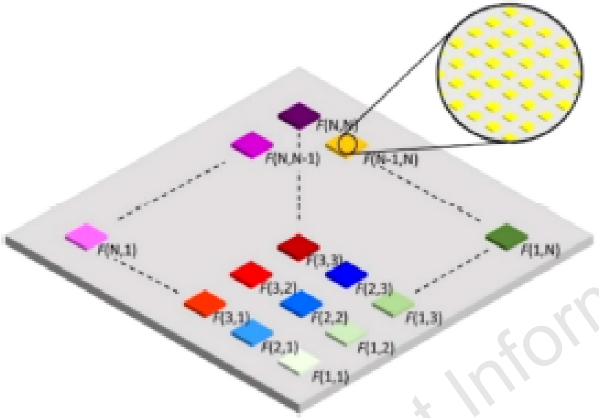

Fig. 15 **Schematic of the filter array in a plasmonic metasurface spectrometer**

Reprinted from Craig et al. (2018), Copyright 2018, with permission from OSA

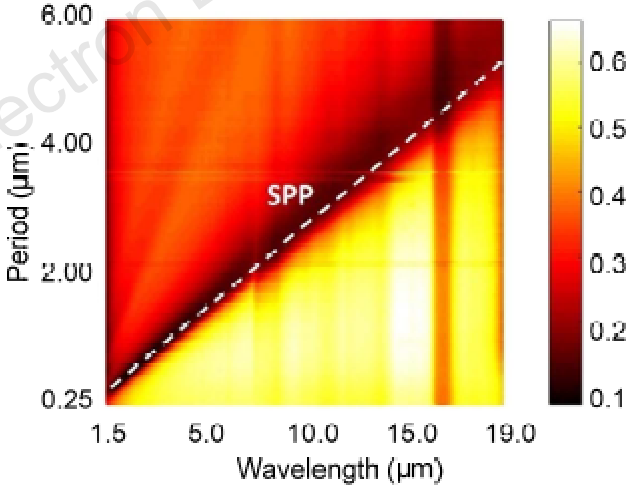

Fig. 16 **Measured transmission spectra for all 116 filters in a plasmonic metasurface spectrometer**

Reprinted from Craig et al. (2018), Copyright 2018, with permission from OSA

Computational spectrometers

5. Plasmonic metasurface spectrometer

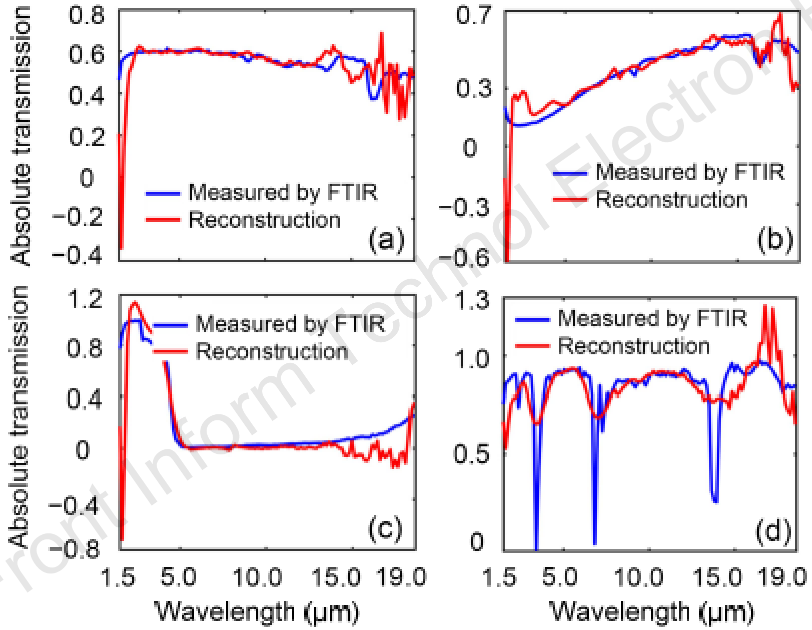

Fig. 17 Reconstruction results of a plasmonic metasurface spectrometer generated by passing light from the globar through double-sided polished undoped silicon (Si) (a), single-sided polished doped Si (b), glass (c), and polyethylene (d)

Reprinted from Craig et al. (2018), Copyright 2018, with permission from OSA

Computational spectrometers

6. Photonic crystal slab spectrometer

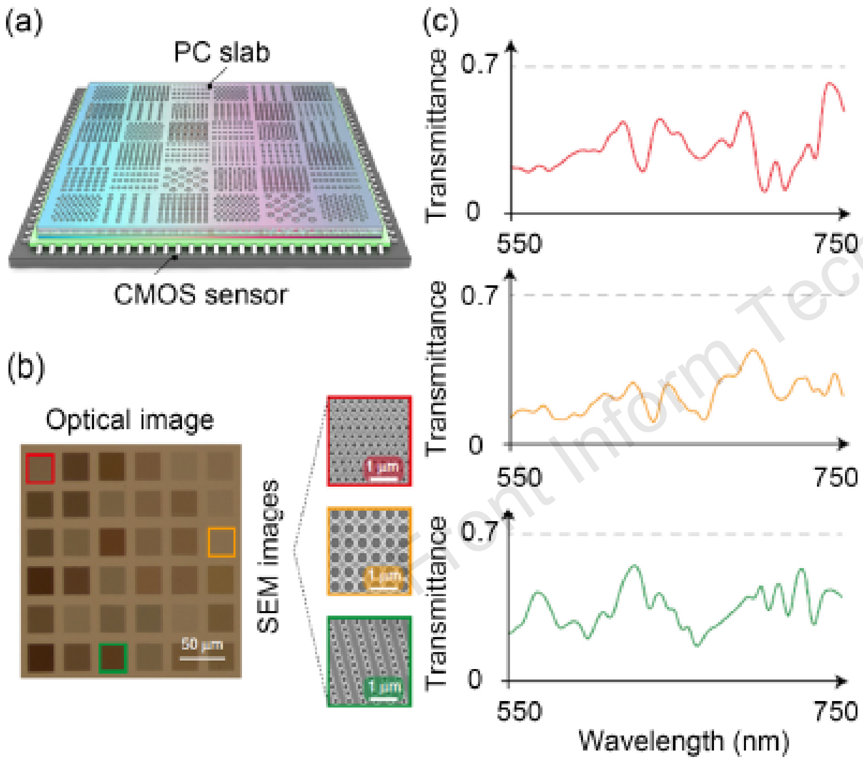

Fig. 18 **Micro-spectrometer based on photonic crystal (PC) slabs: (a) schematic of the spectrometer, which consists of an array of PC slabs with different parameters; (b) optical image of the fabricated 6×6 PC structures; (c) measured transmission spectra *T*(*λ*) of the three structures in (b)**

In (a), these slabs are integrated on top of a CMOS sensor array. In (b), three scanning electron microscopy (SEM) images of selected PC slab structures marked by red, orange, and green frames are shown on the side. In (c), for each PC slab, the corresponding *T*(*λ*) is characterized using a monochromator. References to color refer to the online version of this figure. Reprinted from Wang Z et al. (2019), Copyright 2019, with permission from Springer Nature, licensed under CC BY 4.0

Computational spectrometers

6. Photonic crystal slab spectrometer

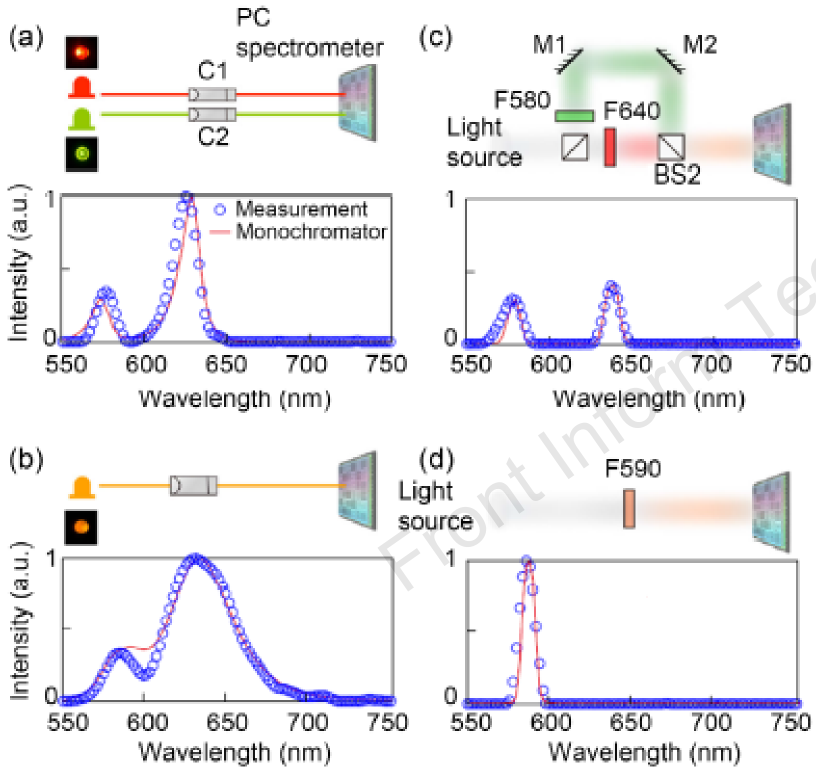

Fig. 19 Recovery of broadband spectra: (a) measurement of the emission spectrum of a combination of two LEDs (green and red); (b) measurement of the emission spectrum of a multimode LED (orange/red); (c) measurement of a white light beam passing through two filters; (d) measurement of a white light beam passing through a single bandpass filter

The appearance color of the filtered light in (d) is the same as that of the recombined light in (c). For all four cases, the measurement results using the PC spectrometer (circled lines) match well the reference spectra obtained by a commercial monochromator (red solid line). M: mirror; F: filter; BS: beam splitter. References to color refer to the online version of this figure. Reprinted from Wang Z et al. (2019), Copyright 2019, with permission from Springer Nature, licensed under CC BY 4.0

Computational spectral imaging

1. Computed tomography imaging spectrometry (CTIS)

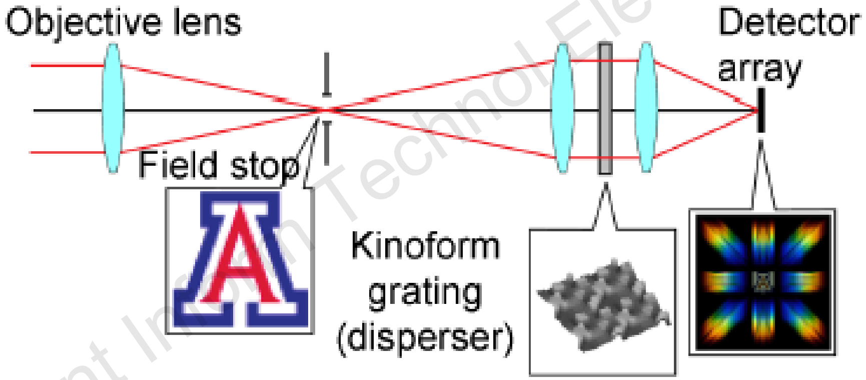

Fig. 20 System layout of a computed tomography imaging spectrometer
Reprinted from Hagen and Kudenov (2013), Copyright 2013, with permission from SPIE, licensed under CC BY 3.0

Computational spectral imaging

2. HyperCam

Goel et al. (2015) designed a product named “HyperCam” for ubiquitous spectral imaging. It has a simple system structure, i.e., a 17-LED light source, a driver board, and a CMOS camera (Photo of the system is available from Goel et al. (2015)). Each part is of low cost and is designed for consumer use. The frame rate goes from 9 to 150 frames/s depending on the number of channels used, and the spatial resolution is 1280×1024.

Computational spectral imaging

3. Coded aperture snapshot spectral imager (CASSI)

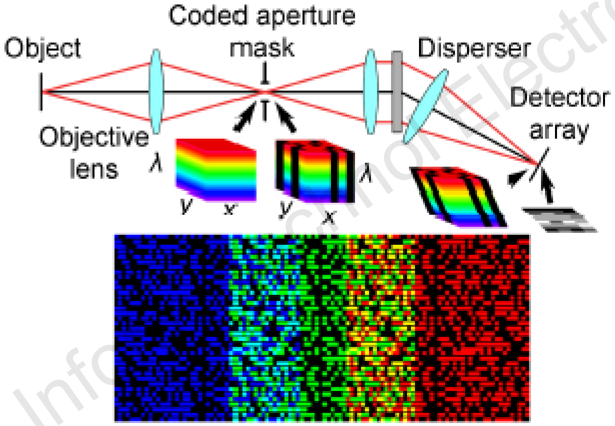

Fig. 21 Schematic of the coded aperture snapshot spectral imager (CASSI) system

Top: system layout for a CASSI, showing only the single-disperser configuration. Bottom: pattern on the detector array due to imaging a coded aperture mask through a disperser for an object that emits only three wavelengths (the wavelengths used in the example image here are the shortest, middle, and longest wavelengths detected by the system). Reprinted from Hagen and Kudenov (2013), Copyright 2013, with permission from SPIE, licensed under CC BY 3.0

Conclusions

- Spectral information acquisition technology has developed rapidly over past decades. These methods are highlighted by their low cost, light weight, and compact enclosures.
- Efforts have been made in recent years for consumer used spectral detection. We believe that the co-design of hardware and the computational algorithm will lead to the wide use of spectral information, and that with the developments of Internet of Things (IoT) and artificial intelligence (AI), ubiquitous spectrometers and spectral imaging will bring benefit to humankind.